Published in final edited form as:
J Med Chem. 2009 August 27; 52(16): 5207–5216. doi:10.1021/jm9005252.

Modern Homology Modeling of G-Protein Coupled Receptors: Which Structural Template to Use?

Juan Carlos Mobarec, **Roberto Sanchez**, and **Marta Filizola***
Department of Structural and Chemical Biology, Mount Sinai School of Medicine, New York, NY.

Abstract

The recent availability in the literature of new crystal structures of inactive G-protein coupled receptors (GPCRs) prompted us to study the extent to which these crystal structures constitute an advantage over the former prototypic rhodopsin template for homology modeling of the transmembrane (TM) region of human class A GPCRs. Our results suggest that better templates than those currently available are required by the majority of these GPCRs to generate homology models that are accurate enough for simple virtual screening aimed at computer-aided drug discovery. Thus, we investigated: 1) which class A GPCRs would have the highest impact as potential templates for homology modeling of other GPCRs, if their structures were solved; and 2) the extent to which multiple-template homology modeling (using all currently available GPCR crystal structures) provides an improvement over single-template homology modeling, as evaluated by the accuracy of rigid protein-flexible ligand docking on these models.

INTRODUCTION

Heptahelical transmembrane (TM) proteins also known as G-protein coupled receptors (GPCRs) are a superfamily of integral membrane proteins whose function is to transmit biological signals from the extracellular milieu toward the cytoplasm, giving rise to signaling cascades that regulate a variety of cellular and physiological functions. The human genome contains around 1000 GPCR sequences 1, 2, which can be classified into five distinct classes (GRAFS system) 1 using phylogenetic trees based on TM helices. Because of experimental difficulties, however, there is a strong imbalance between the number of known GPCR sequences and the number of known structures.

The first crystal structure of a GPCR, i.e. *Bos taurus* Rhodopsin (Bt_Rho), appeared in the literature almost a decade ago [3]. Since bovine rhodopsin is relatively easy to obtain in high quantities, several crystal structures of its 11-cis-retinal-bound ground state [3-9] and of early photointermediates[10-13], including a retinal Schiff base deprotonated state, have been published during the last decade. The first crystal structures of a non-rhodopsin GPCR for diffusible hormones and neurotransmitters, the *Homo sapiens* β2-adrenergic receptor (Hs_Adrb2) bound to partial inverse agonist carazolol [14-16], were obtained at the end of 2007 using two different approaches to stabilize the receptor protein. In the first approach, an antibody fragment (Fab5) generated in detergent from a monoclonal antibody (Mab5) that binds to the third intracellular loop (IC3) of Hs_Adrb2 was used to reduce the dynamic nature

*To whom correspondence should be addressed: Dr. Marta Filizola Department of Structural and Chemical Biology Mount Sinai School of Medicine 1425 Madison Avenue, Box 1677; New York, NY 10029−6574 Tel: 212−659−8690; Fax: 212−849−2456; Email: marta.filizola@mssm.edu.

Supporting Information **Available**: Supporting Information Figures 1-4 and Supporting Information Table 1 are available free of charge via the Internet at http://pubs.acs.org

of this loop, thus facilitating receptor crystallization. The second structure of Hs_Adrb2 was obtained by protein engineering, replacing the IC3 loop sequence from Q230 to S262 with a well folded soluble protein, T4-lysozyme 15. This structure was followed by a third crystal structure of Hs_Adrb2 bound to cholesterol and the partial inverse agonist timolol 17, as well as by a new crystal structure of rhodopsin from *Todarodes pacificus* (Tp_Rho) [18], which exhibited extended TM helices 5 and 6 at the cytoplasmic side and a consequent reduced length for IL3. Another non-rhodopsin GPCR whose crystal structure appeared last year in the literature is a mutant version of β1 adrenergic receptor from *Meleagris gallopavo* (Mg_Adrb1_m23) [19]. This new adrenoceptor structure was obtained by introducing in wild-type receptor six point mutations, whose combination was necessary to stabilize the receptor in a wide range of detergents ideal for crystallization. Crystallization of a lysozyme-fused form of *Homo sapiens* adenosine A2A receptor (Hs_Aa2ar) with antagonist ZM241385 also led to structure determination [20], further supporting the generalization of this crystallization approach to other GPCRs 21. Finally, two crystal structures of ligand-free native bovine opsin 22, 23 with or without a co-crystallized C-terminal peptide derived from the α-subunit of the G-protein transducin have recently appeared in the literature. These structures are unique in that they encompass some of the structural features that have often been attributed to active GPCR conformations [24].

In summary, there are currently 22 crystal structures of inverse agonist-bound class A GPCRs described in the literature [3-20]. However, these structures only cover three GPCR sub-families, and four species, and exhibit high conformational similarity in their TM regions (Figure 1). Thus, more crystal structures of GPCRs in various conformational states are needed to provide detailed insights into GPCR signaling and functional selectivity. Since GPCR structural biology projects seem to require several years of work before a new crystal structure can be solved, homology modeling may be used in the interim to generate models of the GPCR TM regions that 1) exhibit C-α-root mean square deviation (RMSD) values to the putative crystal structure of 2 Å or less, and 2) are suitable for rigid protein-flexible ligand docking. In this work, we investigated the extent to which: 1) current crystal structures of inactive GPCRs are suitable templates for homology modeling of the TM region of other Class A GPCRs, 2) specific GPCRs are better homology modeling templates for the majority of class A GPCRs, and therefore might be of particular value if resolved by X-ray crystallography, and 3) multiple-template homology modeling (using all currently available GPCR crystal structures) may improve the quality of GPCR models, as evaluated by the accuracy of rigid protein-flexible ligand docking on these models.

RESULTS

Inactive GPCR structures differ more in the outer membrane TM segment than in the inner membrane TM segment

We compared all five available inactive 3D structures of GPCRs (Figure 1) together using global pairwise 3D structural alignments of the C-α atoms of their corresponding TM regions to calculate RMSD values (reported in Supporting Information Table 1). A conserved 7TM topology resulted from these calculations (RMSD<2Å), as well as a high similarity among the individual TM helices (Figure 2A). Not surprisingly, the most similar GPCR structures resulted to be Hs_Adrb2 and Mg_Adrb1_m23, which share 68% sequence identity (SI) and an RMSD of 0.6 Å after superposition of 208 corresponding TM C-α atoms. The most different pairs of inactive GPCR structures corresponded to either Bt_Rho – Mg_Adrb1_m23 or Bt_Rho – Hs_Aa2ar (1.8 Å RMSD for any of them, based on the superposition of 192 or 186 corresponding TM C-α atoms, respectively). A detailed analysis of RMSD values calculated for individual helices after global 3D superposition (Supporting Information Table 1) shows that TM6 and TM7 are the most structurally conserved helices in the ten pairs of inactive GPCR

templates (average RMSD ± std = 1.4 ± 0.4 Å for each helix), while TM2 and TM5 are the most structurally divergent helices (2.7 ± 1.0 and 2.8 ± 1.0 Å, respectively), followed by TM1 (2.3 ± 0.9 Å). Extracellular and intracellular views (perpendicular to the membrane) of the structural superposition between the analyzed GPCR structures are shown in Figure 2B. Inspection of this figure suggests that the outer (extracellular) membrane portion of the 7TMs of the five available GPCR templates differs more than their inner (intracellular) membrane region. To measure the extent of this divergence, we calculated for each TM helix the RMSD values of their outer membrane segments separate from their inner membrane side (residue composition of the inner and outer segments are reported in the Methods section). Figure 2C reports the logarithm of the outer/inner membrane RMSD ratio calculated for each helix, with positive values indicating higher structural divergences in the outer membrane portion of the TMs, as shown for TM1, TM2, TM3 and TM4 of the five available GPCR templates. Notably, these findings are in line with the notion of higher divergence in the TM1−4 outer regions of available GPCR crystal structures due to important differences in the mode of binding of different ligands to orthosteric binding pocket sites. In contrast, TM5, TM6 and TM7 exhibited a slightly larger RMSD in the inner membrane side for most of the compared pairs of inactive GPCR structures. This high divergence in the TM5−7 inner parts might be responsible for the recognition of different G-proteins, as particularly evident by comparison between the longer TM5−6 helices of the Gq-activating squid rhodopsin and the shorter TM5−6 helices of the Gt-activating bovine rhodopsin.

Mg_Adrb1_m23 is the most appropriate template for the majority of Class A GPCRs

We calculated the SI between the TM regions of each of the five different inactive GPCR structural templates that are currently available (Bt_Rho, Tp_Rho, Hs_Adrb2, Mg_Adrb1_m23, and Hs_Aa2ar) and our dataset of human Class A GPCRs aligned using conserved functional residues in their TMs. Figure 3 shows the distributions of template:target SI for each template. With the exception of the Bt_Rho's distribution, all others exhibit a maximum closer to 20−30% SI. Based on the suggestion by Forrest and coworkers [25] that acceptable models of the TM regions of membrane proteins may be obtained for template:target SIs of 30% or higher [25], we measured the right-tail area of these distributions (PSAM values; see bar plot in Supporting Information Figure 1). Figure 4 shows an area-weighted Venn diagram of the calculated PSAM values. The higher the calculated PSAM value, the larger the number of human class A GPCR sequences that could be modeled with a certain degree of accuracy using a given GPCR crystal structure as a template. Among the five available inactive structural templates of GPCRs, Mg_Adrb1_m23 (red) or Hs_Adrb2 (blue) (PSAM=18% and 16%, respectively) are calculated to be better templates for the largest fraction of human class A GPCRs than Hs_Aa2ar (gray), Bt_Rho (cyan) or Tp_Rho (yellow) (PSAM = 12%, 2% and 1%, respectively). This did not come as a complete surprise since Mg_Adrb1_m23 and Hs_Adrb2 are members of the large class of amine GPCRs. As shown in Figure 4, the datasets of GPCR sequences that may be built more reliably using Mg_Adrb1_m23 or Hs_Adrb2 overlap almost completely, due to the high sequence similarity between these two templates.

Since several GPCR sequences can exhibit SIs of 30% or higher with more than one single GPCR template, we calculated which of the currently available inactive GPCR crystal structures shared the highest SI with each GPCR target, thus identifying the most appropriate structural template for each GPCR target. Mg_Adrb1_m23 is the most appropriate available template for 16% of the sequences in the human class A GPCR dataset while Hs_Adrb2, Hs_Aa2ar, Bt_Rho and Tp_Rho are the most appropriate templates for 6%, 3%, 2%, and 1% of the targets, respectively (see Supporting Information Figure 2). These percentages include the number of targets that share the same SI with different templates. The human GPCR entry names26 (different colors represent different groups according to the GRAFS classification system1) whose homology modeling would benefit from the use of any available single GPCR

structural template are listed inside the Venn diagram circles shown in Figure 5. Specifically, the GPCR TM regions that could be built reliably using either template (SI>30%) are shown at circle intersections, while the specific sequences that can preferably use one template over others (difference in template:target SI was arbitrarily set up to more than 10%) are listed in the non-intersected areas of the Venn diagram circles depicted in Figure 5.

New crystal structures are needed to model the majority of class A GPCRs

To identify human GPCRs that could be better single structural templates for homology modeling of the largest number of human GPCR sequences, and might therefore be of particular value if resolved by X-ray crystallography, we calculated the template:target SI for each human GPCR sequence in the non-orphan non-olfactory data set, summed all the SI values greater than 30%, and selected those templates that exhibited high SI sums. Somatostatin receptor 5 (SSR5) exhibited the highest SI sum, with a PSAM value of 31%. Hence, determining its crystal structure might have the highest impact on single-template modeling of human GPCRs (77 sequences; see Supporting Information for corresponding list of receptors). Somatostatin receptor 4 (SSR4) (PSAM=30%), and high affinity interleukin-8 receptor B CXCR2 (PSAM=29%) were also identified as potential high-impact templates. A similar calculation carried out on the dataset of class A human orphan and olfactory GPCRs, identified olfactory receptor 10A5 of family 10, subfamily A (O10A5; PSAM=81%), olfactory receptor 4Q3 of family 4 subfamily Q3 (OR4Q3; PSAM=80%), and olfactory receptor 1E1 of family 1, subfamily E (OR1E1; PSAM=79%) as potential high-impact templates.

Impact of multiple-template based models on homology modeling of class A GPCRs

To estimate the accuracy of multiple-template modeling for class A GPCR sequences of unknown structure, we calculated (see Methods section for details) the “Collective Sequence Identity” (CSI) between targets in the human GPCR dataset and a multiple-template model composed of all five currently available inactive GPCR crystal structures. Since CSI values are higher than SI values, we adjusted the CSI cutoff to provide an accuracy equivalent to 2 Å RMSD (Supporting Information Figure 3). The CSI is used here as an indication of the potential structural complementarity of a set of templates toward the receptor to be modeled. The CSI distribution exhibited a $PSAM_{50}$ value of 45% suggesting that, if our estimation of the contribution of multiple templates is correct, almost half class A GPCRs might be modeled with a minimal accuracy around 2 Å using a multiple-template composed of the five available inactive GPCR crystal structures.

To evaluate the ability of multiple-template versus single-template modeling methods to produce accurate GPCR homology models in terms of high structural similarity with their cognate crystal structures, we built homology models of GPCRs with available crystal structures using either single templates or multiple templates (see detailed list, as well as SI and CSI values in Table 1). The latter were built by combining all currently available crystal structures with the exception of the crystal structure of the GPCR under study (Multiple1 in Table 1 and Figure 6). We also considered the case in which structurally similar receptors were eliminated from the multiple-template approach (Multiple2 in Table 1 and Figure 6). For instance, we built homology models of Hs_Adrb2 using: a) either Bt_Rho, or Tp_Rho, or Mg_Adrb1_m23, or Hs_Aa2ar as single templates; and b) a combination of Bt_Rho, Tp_Rho and Hs_Aa2ar with (Multiple1) or without (Multiple 2) Mg_Adrb1_m23. The results of these studies are shown in Figure 6A in terms of model accuracy distributions. Similarly, modeling results for Mg_Adrb1_m23, Hs_Aa2ar, Bt_Rho and Tp_Rho are reported in Figures 6B, 6C, 6D and 6E, respectively. Taken together, the plots of Figure 6 illustrate two points with respect to multiple-template models of inactive GPCR structures: (1) When a template shares high sequence identity with the target (e.g. Mg_Adrb1_m3 for Hs_Adrb2, and vice versa) the inclusion of additional templates does not increase the accuracy of the resulting model (black

line in Figures 6A and 6B); and (2) When all templates share relatively low sequence identity with the target, using them in combination results in a model that is similar or slightly more accurate than the one obtained with any single template (black lines in Figure 6C, 6D, and 6E, and purple lines in 6A and 6B). Thus, no significant improvement was achieved by multiple-template modeling using the currently available GPCR crystal structures compared to single-template modeling. Once again our results suggest that additional GPCR template structures are needed to build accurate homology models for those receptor sequences that are not related to adrenergic, adenosine, or rhodopsin templates.

A comparison of the overall model accuracy (RMSD between the model and its corresponding crystal structure) as a function of single template:target SI or multiple template:target CSI is shown in Supporting Information Figure 3. As expected, and in agreement with previous studies [25, 27, 28], an increased model accuracy (low RMSD) is observed at higher template:target SI/CSI. These studies have shown a linear relationship between SI and accuracy in the data range from 30−100%, which starts to curve from 20% and lower SI values. Our data show that a SI of 30% has an equivalent accuracy for a CSI of 50%, and thus SI and CSI identities would have equivalent accuracies with a 50% cutoff value of CSI.

Single template- vs. multiple template- based models for use in docking experiments

To statistically compare the predictive power of single-template or multiple-template models of Hs_Adrb2 versus the recent Hs_Adrb2 crystal structure (with or without loops) in virtual docking screenings, we built several models of the 7TM region of the receptor, and used them for flexible ligand - rigid protein docking. Specifically, these models, which are listed in Table 2, were based on a) Bt_Rho crystal structure (TM SI=21%), b) Mg_Adrb1_m23 crystal structure (TM SI=68%), c) a combination (Multiple1) of Bt_Rho, Tp_Rho, Mg_Adrb1_m23, and Hs_Aa2ar (TM CSI=77%), and d) a combination (Multiple2) of Bt_Rho, Tp_Rho, and Hs_Aa2ar (TM CSI=48%). Docking of carazolol to either the entire crystal structure of Hs_Adrb2, or the crystal structure of Hs_Adrb2 without loops, or any of the single- or multiple-template models of Hs_Adrb2 listed above was performed according to the protocol described in Methods.

Five different conformations of each single or multiple template model were selected for docking. Specifically, these five conformations differed in the orientation of the side chains within the active site defined as in Surgand et al.[29] Thus, we evaluated the ability of the aforementioned Hs_Adrb2 models to predict the largest population of suitable docking solutions for carazolol (RMSD < 2Å from crystal structure). Specifically, we calculated the percentage (P) of docking solutions with less than 2 Å RMSD from the crystal structure obtained for each single- or multiple template- based models. Our results suggest that all the receptor models produced suitable binding poses (RMSD < 2Å from crystal structure), despite evident differences in the number of accurate predictions.

Supporting Information Figure 4 shows the cumulative percentage of suitable docking solutions achieved using either the crystal structure or the different homology models of Hs_Adrb2. Specifically, The Hs_Adrb2 crystal structure with or without loops resulted in 32% and 60% of suitable binding solutions, respectively, whereas the Bt_Rho-based model of Hs_Adrb2 produced only a few suitable binding solutions (P=0.2%). The results suggest that loops may somehow interfere with the docking process, and that at least in this case, GPCR models without loops may constitute a better alternative for flexible ligand-rigid protein docking. Similarly, models based on Mg_Adrb1_m23 resulted in large populations of suitable binding poses for carazolol (P=29%), whereas Multiple1 and Multiple2 models yielded only 25% and 0.8% accurate docking solutions, respectively. Figure 7 shows the lowest RMSD binding poses identified by molecular docking at the complete Hs_Adrb2 crystal structure (Figure 7A; RMSD=0.86 Å), the Hs_Adrb2 crystal structure without loops (Figure 7B;

RMSD=0.88 Å), the Bt_Rho-based model of Hs_Adrb2 (Figure 7C; RMSD=2.55 Å), the Mg_Adrb1_m23-based model of Hs_Adrb2 (Figure 7D; RMSD=0.66 Å), the Multiple1 model of Hs_Adrb2 (Figure 7E; RMSD=0.98 Å), and the Multiple2 model of Hs_Adrb2 (Figure 7F; RMSD=1.42 Å). Notably, our docking protocol was able to reproduce the crystal solution of carazolol with relatively high accuracy (RMSD < 1 Å) for the complete Hs_Adrb2 crystal structure, the Hs_Adrb2 crystal structure without loops, the Mg_Adrb1_m23-based model of Hs_Adrb2, and the Multiple 1 model of Hs_Adrb2. Slightly higher energy scores resulted from the docking experiment of carazolol at the Hs_Adrb2 crystal structure without loops (data not shown), compared to the values with loops, suggesting that Hs_Adrb2 loops do not play a crucial role in the docking of carazolol to Hs_Adrb2, but their role may be rather related to regulating the accessibility of ligands to the orthosteric binding pocket of GPCRs [30].

DISCUSSION AND CONCLUSIONS

Recent advances in structural biology of GPCRs have shed new light on receptor ligand binding and activation, opening the door to putative improved models of these receptors. We have studied the impact of this new structural information on structure-based drug discovery approaches. Specifically, we have investigated the extent to which current inactive crystal structures of GPCRs are suitable templates to build accurate homology models of the TM region of human class A GPCRs for use in simple structure-based virtual screening aimed at computer-aided drug discovery.

Our results showed that Mg_Adrb1_m23, Hs_Adrb2, and Hs_Aa2ar are suitable templates (Sequence identity >30%) for homology modeling of the 7TMs of 18%, 16% and 12% of non-orphan non-olfactory human class A GPCRs, respectively, while Bt_Rho and Tp_Rho can significantly contribute to the modeling of only 2% and 1% of GPCRs, respectively. Despite the larger number of GPCR sequences (mostly amine receptors) that can be modeled with higher confidence using either Hs_Adrb2 or Mg_Adrb1_m23 crystal structures as single templates, as compared with adenosine and rhodopsin structures, our results suggest that the majority of class A GPCRs still need better structural templates than those currently available to obtain homology models that, together with appropriate docking tools and scoring functions, may enhance computer-assisted drug design. Our results suggest that SSR5, SSR4 or CXCR2 might be the most desirable GPCRs for future crystallization since a larger number of non-olfactory non-orphan human class A GPCRs (~30% of the dataset) exhibit a SI higher than 30% with respect to any of these potential new templates, and might therefore benefit from the use of these templates for homology modeling. Similarly, in the case of olfactory and orphan human class A GPCRs a much larger number of GPCRs (80% of olfactory and orphan receptors) could be built more reliably if crystal structures of O10A5, OR4Q3, or OR1E1 were available as templates.

Albeit small, variations in the individual TM helices revealed by the recent rhodopsin and non-rhodopsin inactive crystal structures appear to affect the ability of a ligand to bind in a correct orientation, as predicted by flexible ligand-rigid protein virtual screening approaches. Hence, the need to improve the quality of homology models of GPCRs using more appropriate templates. We showed that rhodopsin-based homology models of the distant homologous Hs_Adrb2 fail to predict correct ligand-binding poses using simple docking tools and scoring functions. Nevertheless, the lack of loops in the Hs_Adrb2 crystal structure did not prevent us from identifying accurate binding poses for carazolol (RMSD<2Å from crystal structure), suggesting once again [31] that some GPCR models built without extracellular loops may constitute a viable alternative for virtual docking experiments.

To try to improve the quality of GPCR models, we explored the possibility of using multiple templates for homology modeling. Thus, we estimated the contribution of all currently

available GPCR structures to the multiple-template modeling of a given target using a calculated CSI value. Our analysis suggests that the use of multiple templates can provide similar or slightly improved models of the TM region of GPCRs when compared to receptor models obtained using single templates. Model accuracy is expected to improve as more GPCR structures become available, depending on the collective identity of the different multiple templates that are taken into account.

Although it is reasonable to expect that multiple-template models would exhibit a higher predictive power in flexible ligand-rigid protein docking experiments, accuracy is a global measure of the properties of the complete structure, while for docking purposes the correct orientation of side chains within the binding pocket may be the most important aspect [31]. Accordingly, we were able to find, with high frequency, suitable docking solutions of carazolol (RMSD<2Å from the crystal structure binding pose) only in docking experiments that either used the Hs_Adrb2 crystal structure or models based on highly similar templates such as Mg_Adrb1_m23. Docking experiments that rely on models based on lower similarity templates (≤ 35% sequence identity) showed a reduced predictive ability, also when combining multiple templates. Availability of additional GPCR crystal structures that can serve as templates in the 35−65% sequence identity range will be required to test the ability of multiple template modeling to significantly impact the accuracy of GPCR homology models for docking studies.

EXPERIMENTAL SECTION

Nomenclature and residue numbering

Each GPCR template is indicated by the initials of the binomial nomenclature used for naming species followed by the generic or abbreviated name of the receptor. For instance, *Bos taurus* rhodopsin is indicated by Bt_Rho, while *Meleagris gallopavo* β1 adrenergic receptor mutant m23 is indicated by Mg_Adrb1_m23. Residues are numbered both according to their positions in the GPCR sequence and to the two-number identifier by Ballesteros & Weinstein [32] reported as a superscript. Specifically, this two-number identifier consists of the TM helix number (from 1 to 7) and the residue position in the helix relative to its most conserved residue (assigned index of 50) with numbers decreasing toward the helix N-terminus and increasing toward its C-terminus.

Sequence dataset

The aligned amino acid sequences of the TM regions of 614 human class A GPCRs were extracted from the GPCRDB release 10.0 (June 2006) [33]. These sequences, whose GPCRDB alignment is based on the highly conserved functional residues in each TM segment were visually inspected, and then separated into two distinct data sets containing either non-orphan non-olfactory class A GPCR receptors (249 sequences) or orphan and olfactory class A GPCR receptors (365 sequences). The TM sequences of each GPCR were extracted and analyzed as both individual helices and helical bundles. The analysis reported hereafter is based on the 249 sequence dataset of non-orphan non-olfactory class A human GPCR receptors unless otherwise specified.

Template dataset

. Five inverse agonist-bound GPCR crystal structures were taken into account as templates for homology modeling of inactive GPCRs (Figure 1): Bt_Rho (1U19, chain A, 2.2 Å resolution 7), Tp_Rho (2Z73, chain A, 2.5 Å resolution 18), Hs_Adrb2 (2RH1, chain A, 2.4 Å resolution 15), Mg_Adrb1_m23 (2VT4, chain B, 2.7 Å resolution 19), and Hs_ Aa2ar (3EML, chain A, 2.6 Å resolution 20).

Structural comparison of crystal structures

The RMSD of the C-α atoms was used to measure the structural similarity between the TM regions of pairs of available GPCR inactive templates following their structural alignment with the command ALIGN3D of MODELLER 34. Outer and inner membrane sides of the TM helices were approximately assigned based on an average structure resulting from equilibrated molecular dynamics simulations of Bt_Rho in an explicit lipid-water environment [35]. Specifically, the following segments were chosen: residues 1.30−1.43 (outer) and 1.44−1.59 (inner) for TM1, 2.50−2.67 (outer) and 2.38−2.49 (inner) for TM2, 3.33−3.37 (outer) and 3.38 −3.55 (inner) for TM3, 4.51−4.63 (outer) and 4.39−4.50 (inner) for TM4, 5.36−5.48 (outer) and 5.49−5.68 (inner) for TM5, 6.47−6.60 (outer) and 6.29−6.46 (inner) for TM6, and 7.32 −7.46 (outer) and 7.47−7.55 (inner) for TM7.

Percentage of Sequences for Accurate Models (PSAM)

was defined as the percentage of target TM sequences in a given dataset that share SI higher than 30% with a given structural template. Because of the relationship between sequence similarity and model accuracy in membrane proteins [25], PSAM represents the percentage of targets that are expected to have models with accuracy lower than 2 Å RMSD (C-α atoms) (area in the right-tail of template:target SI distributions). Additional calculations carried out using a SI cutoff of 25% yielded the same conclusions inferred by the 30% cutoff.

Potential high-impact templates for homology modeling of GPCRs

To select which class A GPCR might be a better template for homology modeling than currently available templates, we first calculated the SI between the TM region of each of the currently available GPCR crystal structures and the TM regions of GPCRs in the dataset. The highest sum of the calculated SIs greater than 30% was then selected, and the top ranked receptors were reported together with their PSAM value.

Template Alignment and TM Model Building

Models of the TM regions were calculated using the sequence alignments and the template structures described above as inputs to the default ‘model’ routine of the MODELLER v8.2 software [34]. Either single or multiple templates were considered. Every target sequence with an available 3D crystallographic structure was subject to homology modeling using either a single template (other than their own crystal structures) or multiple templates (with the exception of their own crystal structure or crystal structures from the same GPCR sub-family). One thousand models were generated for each template:target modeling experiment. The Rosetta scoring function [36], which was recently shown to be a suitable scoring function for membrane protein homology models 37, was used to select one of the models for docking experiments.

Accuracy of the models

The accuracy of the TM models, i.e. the structural similarity between a model and the crystallographic structure of the target was measured by RMSD, using the SUPERPOSE command of MODELLER [34] without setting a specific cutoff value.

Sequence-based evaluation of multiple-templates

Multiple-templates were obtained by using the sequences of three or more inactive GPCR crystal structures simultaneously. Specifically, we estimated the potential contribution of different sets of GPCR templates to the modeling of a given GPCR target by calculating a ‘collective sequence identity’ (CSI) parameter. CSI is obtained by counting the number of alignment positions at which at least one template residue is identical to the target residue, and

dividing this number by the length of the alignment. Notably, the relationship between SI and CSI is not clear.

Recent studies 25, [38] using a dataset of thousands of single-template models of globular and membrane proteins of known structure suggested a non-linear relationship between SI and structural accuracy. However, the data for transmembrane proteins (without considering loops) can be represented by a linear relationship in the SI range between 30−100% [25]. It is possible that CSI values would follow a similar trend (see Supporting Information Figure 3). Our limited number of single template- and multiple template-based models that can be built using current crystal structures of GPCRs provide accuracy values that are in agreement with those published for membrane proteins [25] and globular proteins [38]. The CSI values are displaced to the right in the CSI accuracy plot of Supporting Information Figure 3, and we observe that a CSI value of 50% corresponds to an accuracy of approximately 2 Å RMSD. We used this PSAM cutoff of 50% ($PSAM_{50}$) to estimate the contribution of the five representative GPCR crystal structures to multiple template-based models of class A GPCRs, and therefore to obtain a PSAM value for multiple-templates that is comparable in accuracy to those of single template-based models.

Molecular Docking

Rigid protein-flexible ligand docking was carried out with AUTODOCK v3.0 [39] to predict binding modes of carazolol into the orthosteric binding pocket of the Hs_Adbr2 crystal structure, multiple-template based models, and single-template based models listed in Table 2. For any given template, five models were selected. Specifically, one model was selected based on Rosetta scoring function, while the other four models were based on the different orientation of the side chains within a predefined active site,[29] as evaluated by RMSD. Structural parameters for carazolol, Hs_Adrb2, Hs_Adrb2-Rho, Hs_Adrb2_Adrb1, Hs_Adrb2_Multiple1, and Hs_Adrb2_Multiple2 were assigned with Autodock Tools (ADT) [40]. A reference grid box for docking was set up using the Hs_Adbr2 crystal structure, and was centered in the middle of its TM bundle (4.38 Å from the Cα atom of $F193^{5.32}$, 4.69 Å from the OH group of $Y308^{7.35}$, and 4.0 Å from the amide oxygen of $N312^{7.39}$), featuring a size of 88x86x68 points with a grid spacing of 0.375 Å. This box surrounded the Hs_Adbr2 orthosteric site and allowed for free ligand rotation and displacement in each docking system. A genetic algorithm protocol was selected for an exhaustive conformational sampling of carazolol within the proteins. Specifically, we used a starting population of 150 random positions of the ligand into its grid box, and a total number of 2,500,000 docking evaluations. We performed 100 different docking experiments for each Hs_Adrb2 model. A larger number of docking experiments (data not shown) was performed using the Hs_Adrb2 crystal structure to check for consistency. Docking accuracy was assessed by calculating the RMSD between all heavy atoms of carazolol in the X-ray crystal structure (2RH1) and the binding poses resulting from each docking experiment.

Supplementary Material

Refer to Web version on PubMed Central for supplementary material.

Acknowledgments

This work was supported by NIH grants DA020032 and DA026434 from the National Institute on Drug Abuse.

Abbreviations List

Bt_Rho	*Bos Taurus* Rhodopsin

CSI	Collective Sequence Identity
CXCR2	interleukin-8 receptor B
GPCR	G-Protein Coupled Receptor
Hs_Aa2ar	*Homo sapiens* Adenosine A2A receptor
Hs_Adrb2	*Homo sapiens* β2-adrenergic receptor
Mg_Adrb1_m23	*Meleagris gallopavo* β1-adrenergic receptor
O10A5	olfactory receptor 10A5 of family 10 subfamily A
OR4Q3	olfactory receptor 4Q3 of family 4 subfamily Q3
OR1E1	olfactory receptor 1E1 of family 1 subfamily E
P	percentage
PSAM	Percentage of Sequences for Accurate Models
RMSD	root mean square deviation
SI	Sequence Identity
SSR5	Somatostatin receptor 5
SSR4	Somatostatin receptor 4
TM	transmembrane
Tp_Rho	*Todarodes pacificus* Rhodopsin

REFERENCES

1. Fredriksson R, Lagerstrom MC, Lundin LG, Schioth HB. The G-protein-coupled receptors in the human genome form five main families. Phylogenetic analysis, paralogon groups, and fingerprints. Mol Pharmacol 2003;63(6):1256–1272. [PubMed: 12761335]
2. Venter JC, Adams MD, Myers EW, Li PW, Mural RJ, Sutton GG, Smith HO, Yandell M, Evans CA, Holt RA, Gocayne JD, Amanatides P, Ballew RM, Huson DH, Wortman JR, Zhang Q, Kodira CD, Zheng XH, Chen L, Skupski M, Subramanian G, Thomas PD, Zhang J, Gabor Miklos GL, Nelson C, Broder S, Clark AG, Nadeau J, McKusick VA, Zinder N, Levine AJ, Roberts RJ, Simon M, Slayman C, Hunkapiller M, Bolanos R, Delcher A, Dew I, Fasulo D, Flanigan M, Florea L, Halpern A, Hannenhalli S, Kravitz S, Levy S, Mobarry C, Reinert K, Remington K, Abu-Threideh J, Beasley E, Biddick K, Bonazzi V, Brandon R, Cargill M, Chandramouliswaran I, Charlab R, Chaturvedi K, Deng Z, Di Francesco V, Dunn P, Eilbeck K, Evangelista C, Gabrielian AE, Gan W, Ge W, Gong F, Gu Z, Guan P, Heiman TJ, Higgins ME, Ji RR, Ke Z, Ketchum KA, Lai Z, Lei Y, Li Z, Li J, Liang Y, Lin X, Lu F, Merkulov GV, Milshina N, Moore HM, Naik AK, Narayan VA, Neelam B, Nusskern D, Rusch DB, Salzberg S, Shao W, Shue B, Sun J, Wang Z, Wang A, Wang X, Wang J, Wei M, Wides R, Xiao C, Yan C, Yao A, Ye J, Zhan M, Zhang W, Zhang H, Zhao Q, Zheng L, Zhong F, Zhong W, Zhu S, Zhao S, Gilbert D, Baumhueter S, Spier G, Carter C, Cravchik A, Woodage T, Ali F, An H, Awe A, Baldwin D, Baden H, Barnstead M, Barrow I, Beeson K, Busam D, Carver A, Center A, Cheng ML, Curry L, Danaher S, Davenport L, Desilets R, Dietz S, Dodson K, Doup L, Ferriera S, Garg N, Gluecksmann A, Hart B, Haynes J, Haynes C, Heiner C, Hladun S, Hostin D, Houck J, Howland T, Ibegwam C, Johnson J, Kalush F, Kline L, Koduru S, Love A, Mann F, May D, McCawley S, McIntosh T, McMullen I, Moy M, Moy L, Murphy B, Nelson K, Pfannkoch C, Pratts E, Puri V, Qureshi H, Reardon M, Rodriguez R, Rogers YH, Romblad D, Ruhfel B, Scott R, Sitter C, Smallwood M, Stewart E, Strong R, Suh E, Thomas R, Tint NN, Tse S, Vech C, Wang G, Wetter J, Williams S, Williams M, Windsor S, Winn-Deen E, Wolfe K, Zaveri J, Zaveri K, Abril JF, Guigo R, Campbell MJ, Sjolander KV, Karlak B, Kejariwal A, Mi H, Lazareva B, Hatton T, Narechania A, Diemer K, Muruganujan A, Guo N, Sato S, Bafna V, Istrail S, Lippert R, Schwartz R, Walenz B, Yooseph S, Allen D, Basu A, Baxendale J, Blick L, Caminha M, Carnes-Stine J, Caulk P, Chiang YH, Coyne M, Dahlke C, Mays

A, Dombroski M, Donnelly M, Ely D, Esparham S, Fosler C, Gire H, Glanowski S, Glasser K, Glodek A, Gorokhov M, Graham K, Gropman B, Harris M, Heil J, Henderson S, Hoover J, Jennings D, Jordan C, Jordan J, Kasha J, Kagan L, Kraft C, Levitsky A, Lewis M, Liu X, Lopez J, Ma D, Majoros W, McDaniel J, Murphy S, Newman M, Nguyen T, Nguyen N, Nodell M, Pan S, Peck J, Peterson M, Rowe W, Sanders R, Scott J, Simpson M, Smith T, Sprague A, Stockwell T, Turner R, Venter E, Wang M, Wen M, Wu D, Wu M, Xia A, Zandieh A, Zhu X. The sequence of the human genome. Science 2001;291(5507):1304–1351. [PubMed: 11181995]

3. Palczewski K, Kumasaka T, Hori T, Behnke CA, Motoshima H, Fox BA, Le Trong I, Teller DC, Okada T, Stenkamp RE, Yamamoto M, Miyano M. Crystal structure of rhodopsin: A G protein-coupled receptor. Science 2000;289(5480):739–745. [PubMed: 10926528]
4. Stenkamp RE. Alternative models for two crystal structures of bovine rhodopsin. Acta Crystallogr D Biol Crystallogr 2008;D64(Pt 8):902–904. [PubMed: 18645239]
5. Li J, Edwards PC, Burghammer M, Villa C, Schertler GF. Structure of bovine rhodopsin in a trigonal crystal form. J Mol Biol 2004;343(5):1409–1438. [PubMed: 15491621]
6. Okada T, Fujiyoshi Y, Silow M, Navarro J, Landau EM, Shichida Y. Functional role of internal water molecules in rhodopsin revealed by X-ray crystallography. Proc Natl Acad Sci U S A 2002;99(9): 5982–5987. [PubMed: 11972040]
7. Okada T, Sugihara M, Bondar AN, Elstner M, Entel P, Buss V. The retinal conformation and its environment in rhodopsin in light of a new 2.2 A crystal structure. J Mol Biol 2004;342(2):571–583. [PubMed: 15327956]
8. Teller DC, Okada T, Behnke CA, Palczewski K, Stenkamp RE. Advances in determination of a high-resolution three-dimensional structure of rhodopsin, a model of G-protein-coupled receptors (GPCRs). Biochemistry 2001;40(26):7761–7772. [PubMed: 11425302]
9. Standfuss J, Xie G, Edwards PC, Burghammer M, Oprian DD, Schertler GF. Crystal structure of a thermally stable rhodopsin mutant. J Mol Biol 2007;372(5):1179–1188. [PubMed: 17825322]
10. Nakamichi H, Buss V, Okada T. Photoisomerization mechanism of rhodopsin and 9-cis-rhodopsin revealed by x-ray crystallography. Biophys J 2007;92(12):L106–108. [PubMed: 17449675]
11. Nakamichi H, Okada T. Local peptide movement in the photoreaction intermediate of rhodopsin. Proc Natl Acad Sci U S A 2006;103(34):12729–12734. [PubMed: 16908857]
12. Nakamichi H, Okada T. Crystallographic analysis of primary visual photochemistry. Angew Chem Int Ed Engl 2006;45(26):4270–4273. [PubMed: 16586416]
13. Salom D, Lodowski DT, Stenkamp RE, Le Trong I, Golczak M, Jastrzebska B, Harris T, Ballesteros JA, Palczewski K. Crystal structure of a photoactivated deprotonated intermediate of rhodopsin. Proc Natl Acad Sci U S A 2006;103(44):16123–16128. [PubMed: 17060607]
14. Rasmussen SG, Choi HJ, Rosenbaum DM, Kobilka TS, Thian FS, Edwards PC, Burghammer M, Ratnala VR, Sanishvili R, Fischetti RF, Schertler GF, Weis WI, Kobilka BK. Crystal structure of the human beta2 adrenergic G-protein-coupled receptor. Nature 2007;450(7168):383–387. [PubMed: 17952055]
15. Cherezov V, Rosenbaum DM, Hanson MA, Rasmussen SG, Thian FS, Kobilka TS, Choi HJ, Kuhn P, Weis WI, Kobilka BK, Stevens RC. High-resolution crystal structure of an engineered human beta2-adrenergic G protein-coupled receptor. Science 2007;318(5854):1258–1265. [PubMed: 17962520]
16. Rosenbaum DM, Cherezov V, Hanson MA, Rasmussen SG, Thian FS, Kobilka TS, Choi HJ, Yao XJ, Weis WI, Stevens RC, Kobilka BK. GPCR engineering yields high-resolution structural insights into beta2-adrenergic receptor function. Science 2007;318(5854):1266–1273. [PubMed: 17962519]
17. Hanson MA, Cherezov V, Griffith MT, Roth CB, Jaakola VP, Chien EY, Velasquez J, Kuhn P, Stevens RC. A specific cholesterol binding site is established by the 2.8 A structure of the human beta2-adrenergic receptor. Structure 2008;16(6):897–905. [PubMed: 18547522]
18. Murakami M, Kouyama T. Crystal structure of squid rhodopsin. Nature 2008;453(7193):363–367. [PubMed: 18480818]
19. Warne T, Serrano-Vega MJ, Baker JG, Moukhametzianov R, Edwards PC, Henderson R, Leslie AG, Tate CG, Schertler GF. Structure of a beta1-adrenergic G-protein-coupled receptor. Nature 2008;454 (7203):486–491. [PubMed: 18594507]

20. Jaakola VP, Griffith MT, Hanson MA, Cherezov V, Chien EY, Lane JR, Ijzerman AP, Stevens RC. The 2.6 angstrom crystal structure of a human A2A adenosine receptor bound to an antagonist. Science 2008;322(5905):1211–1217. [PubMed: 18832607]
21. Hanson MA, Stevens RC. Discovery of New GPCR Biology: One Receptor Structure at a Time. Structure 2009;17(1):8–14. [PubMed: 19141277]
22. Scheerer P, Park JH, Hildebrand PW, Kim YJ, Krauss N, Choe HW, Hofmann KP, Ernst OP. Crystal structure of opsin in its G-protein-interacting conformation. Nature 2008;455(7212):497–502. [PubMed: 18818650]
23. Park JH, Scheerer P, Hofmann KP, Choe HW, Ernst OP. Crystal structure of the ligand-free G-protein-coupled receptor opsin. Nature 2008;454(7201):183–187. [PubMed: 18563085]
24. Schwartz TW, Hubbell WL. Structural biology: A moving story of receptors. Nature 2008;455(7212): 473–474. [PubMed: 18818642]
25. Forrest LR, Tang CL, Honig B. On the accuracy of homology modeling and sequence alignment methods applied to membrane proteins. Biophys J 2006;91(2):508–517. [PubMed: 16648166]
26. The universal protein resource (UniProt). Nucleic Acids Res 2008;36(Database issue):D190–195. [PubMed: 18045787]
27. Eyrich VA, Marti-Renom MA, Przybylski D, Madhusudhan MS, Fiser A, Pazos F, Valencia A, Sali A, Rost B. EVA: continuous automatic evaluation of protein structure prediction servers. Bioinformatics 2001;17(12):1242–1243. [PubMed: 11751240]
28. Sanchez R, Sali A. Large-scale protein structure modeling of the Saccharomyces cerevisiae genome. Proc Natl Acad Sci U S A 1998;95(23):13597–13602. [PubMed: 9811845]
29. Surgand JS, Rodrigo J, Kellenberger E, Rognan D. A chemogenomic analysis of the transmembrane binding cavity of human G-protein-coupled receptors. Proteins 2006;62(2):509–538. [PubMed: 16294340]
30. Lefkowitz RJ, Sun JP, Shukla AK. A crystal clear view of the beta2-adrenergic receptor. Nat Biotechnol 2008;26(2):189–191. [PubMed: 18259173]
31. Costanzi S. On the applicability of GPCR homology models to computer-aided drug discovery: a comparison between in silico and crystal structures of the beta2-adrenergic receptor. J Med Chem 2008;51(10):2907–2914. [PubMed: 18442228]
32. Ballesteros, J.; Weinstein, H. Integrated methods for the construction of three dimensional models and computational probing of structure function relations in G protein-coupled receptors. Vol. 25. Academic Press; San Diego, CA: 1995. p. 366-428.
33. Horn F, Bettler E, Oliveira L, Campagne F, Cohen FE, Vriend G. GPCRDB information system for G protein-coupled receptors. Nucleic Acids Res 2003;31(1):294–297. [PubMed: 12520006]
34. Sali A, Blundell TL. Comparative protein modelling by satisfaction of spatial restraints. J Mol Biol 1993;234(3):779–815. [PubMed: 8254673]
35. Filizola M, Wang SX, Weinstein H. Dynamic models of G-protein coupled receptor dimers: indications of asymmetry in the rhodopsin dimer from molecular dynamics simulations in a POPC bilayer. J Comput Aided Mol Des 2006;20(7-8):405–416. [PubMed: 17089205]
36. Rohl CA, Strauss CE, Misura KM, Baker D. Protein structure prediction using Rosetta. Methods Enzymol 2004;383:66–93. [PubMed: 15063647]
37. Gao C, Stern HA. Scoring function accuracy for membrane protein structure prediction. Proteins 2007;68(1):67–75. [PubMed: 17407162]
38. Chakravarty S, Godbole S, Zhang B, Berger S, Sanchez R. Systematic analysis of the effect of multiple templates on the accuracy of comparative models of protein structure. BMC Struct Biol 2008;8:31. [PubMed: 18631402]
39. Morris GM, Goodsell DS, Halliday RS, Huey R, Hart WE, Belew RK, Olson AJ. Automated Docking using a Lamarckian Genetic Algorithm and Empirical Binding Free Energy Function. J. Computational Chemistry 1998;19:1639–1662.
40. Sanner MF. Python: a programming language for software integration and development. J Mol Graph Model 1999;17(1):57–61. [PubMed: 10660911]

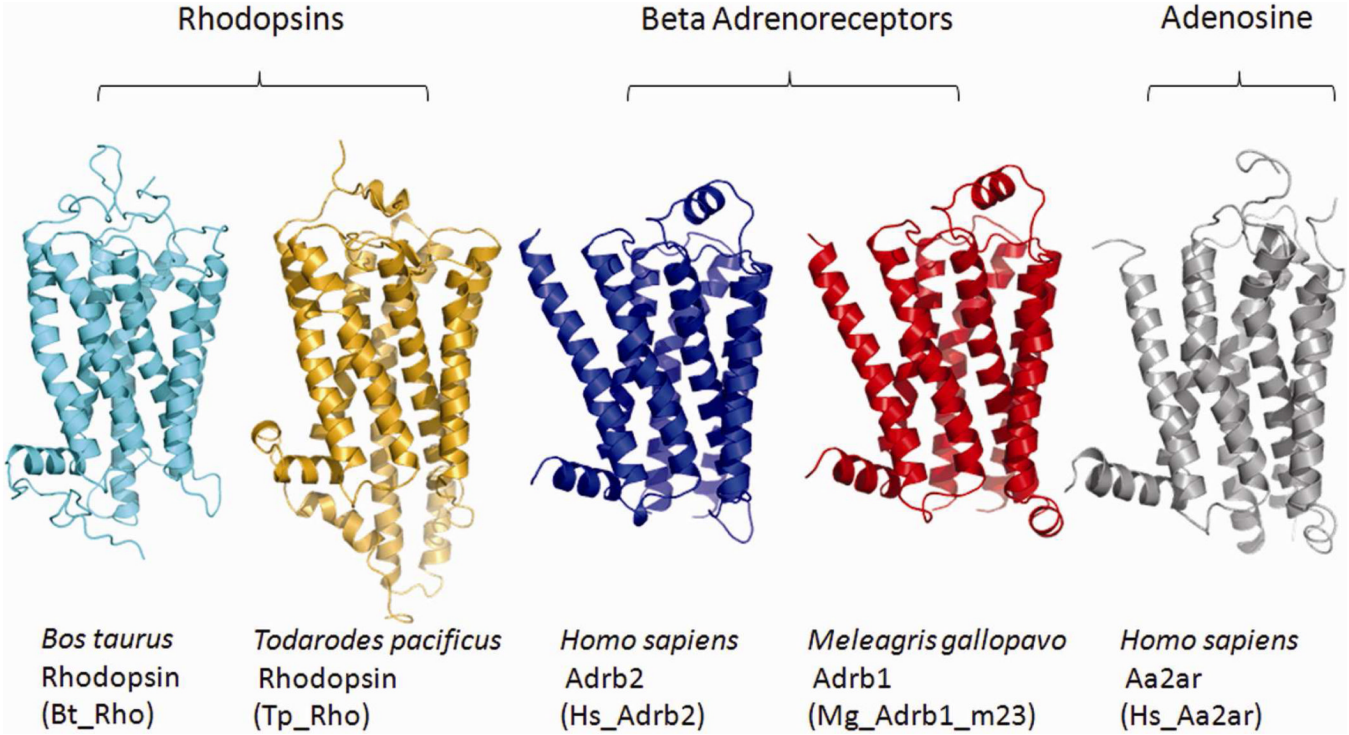

Figure 1.
Representative inactive GPCR crystal structures. Bt_Rho, Tp_Rho, Hs_Adrb2, Mg_Adrb1_m23, and Hs_Aa2ar are shown in cyan, yellow, blue, red, and gray colors, respectively.

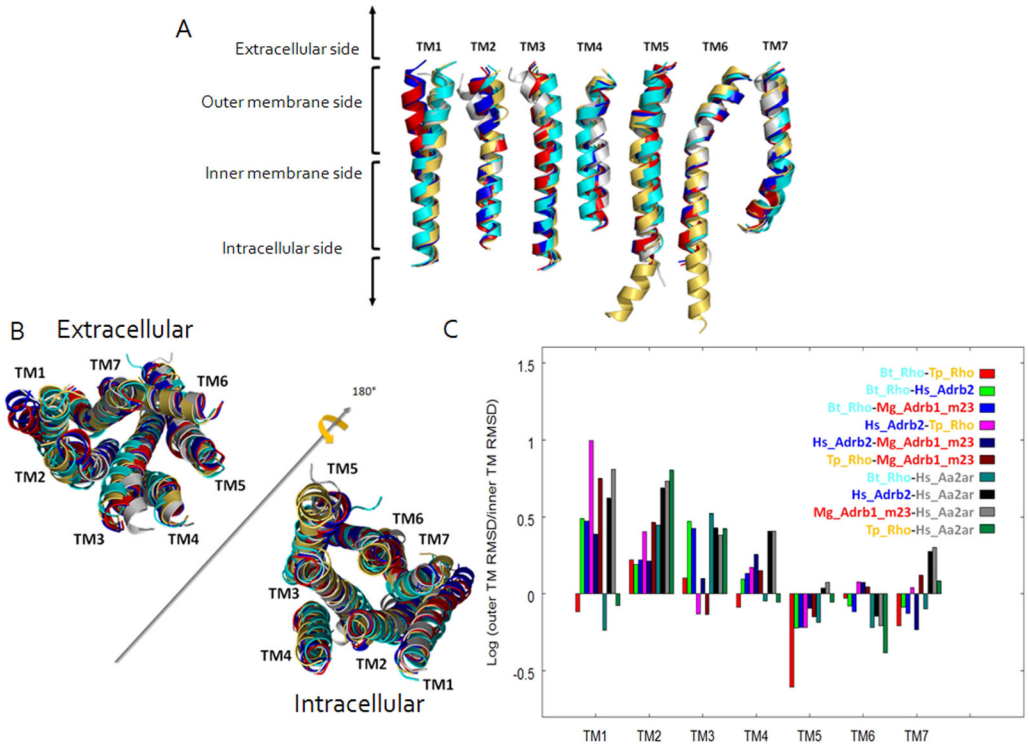

Figure 2.

Superposition of representative inactive GPCR crystal structures. (A) Vertical views of multiple aligned individual TM helices. Black brackets show an approximate representation of extracellular, outer membrane, inner membrane, and intracellular sides of a GPCR. (B) Superimposed outer and inner membrane segments. (C) Calculated log of the ratios of outer/inner membrane RMSD values.

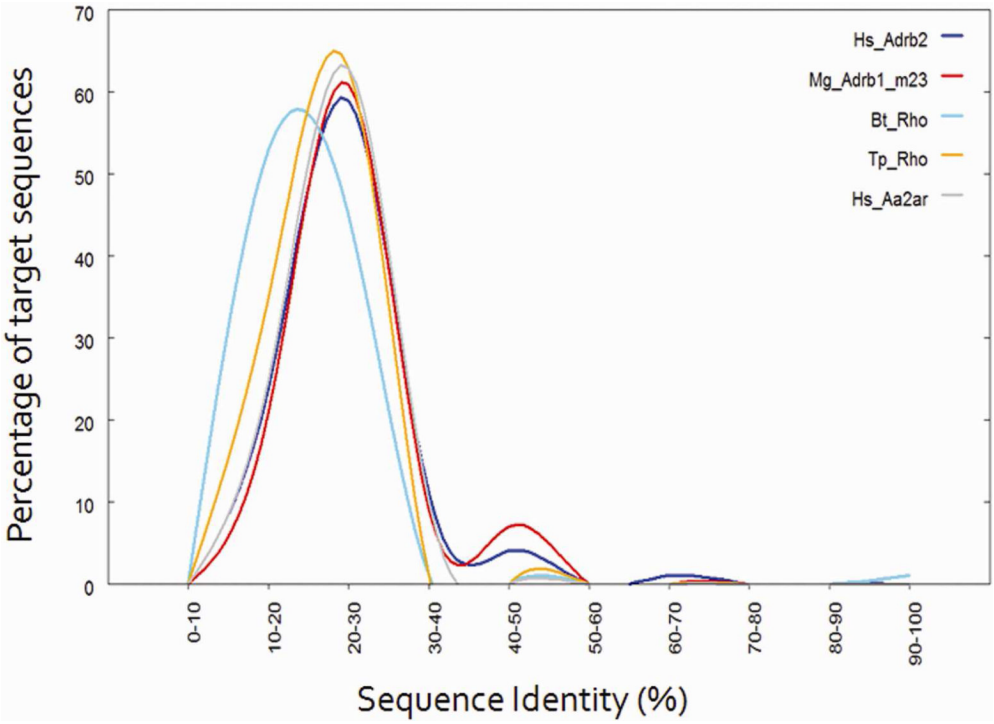

Figure 3.
Template:target Sequence Identity (SI) distributions. SI distributions of available crystal structures Hs_Adrb2, Mg_Adrb1_m23, Hs_Aa2ar, Bt_Rho, Tp_Rho are shown in blue, red, gray, cyan, and yellow, respectively.

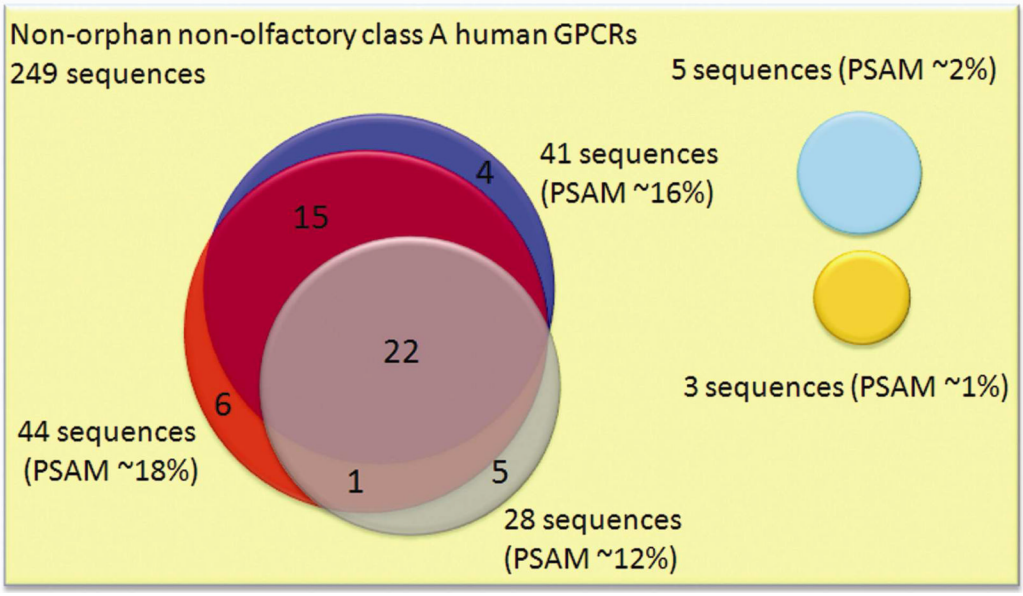

Figure 4.

Area-weighted Venn diagram of the logical relationships between the PSAM values for each template over the entire TM region. The pale yellow rectangle represents the totality of non-orphan non-olfactory class A GPCRs. Coloring of circles as in Figure 3.

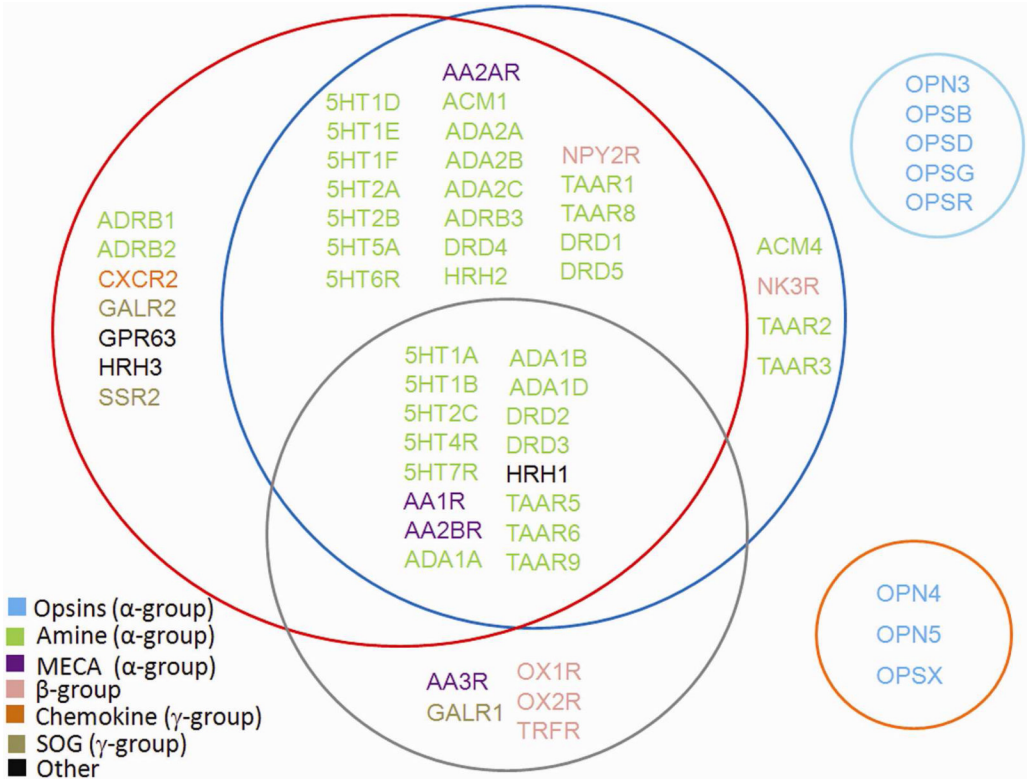

Figure 5.

Venn diagram of human GPCR entry names [26] whose homology modeling would benefit from the use of the available templates. The GPCRs that could be built using either template are shown at circle intersections, while the specific sequences that would be better modeled using one specific template are within circles. Sequences with identity difference greater than 10% between available targets are placed into template exclusive areas in the diagram. The color code of the circles is the same as in Figure 1. Entry names were color coded according to the GRAFS classification system[1]: cyan for the opsin receptor cluster, green for the amine receptor cluster, purple for the MECA (Melanocortin, Endotelial differentiation, Cannabinoid, and Adenosine binding receptors) receptor cluster, pink for the β-group of rhodopsin receptors, orange for the chemokine receptors, brown for the SOG group (Somatostatin, Opioid, GALRs-GPRs), and black for all other receptors outside known groups. Entry names of receptors with a SI lower than 30% in their TM helices with respect to known GPCR structures are not shown.

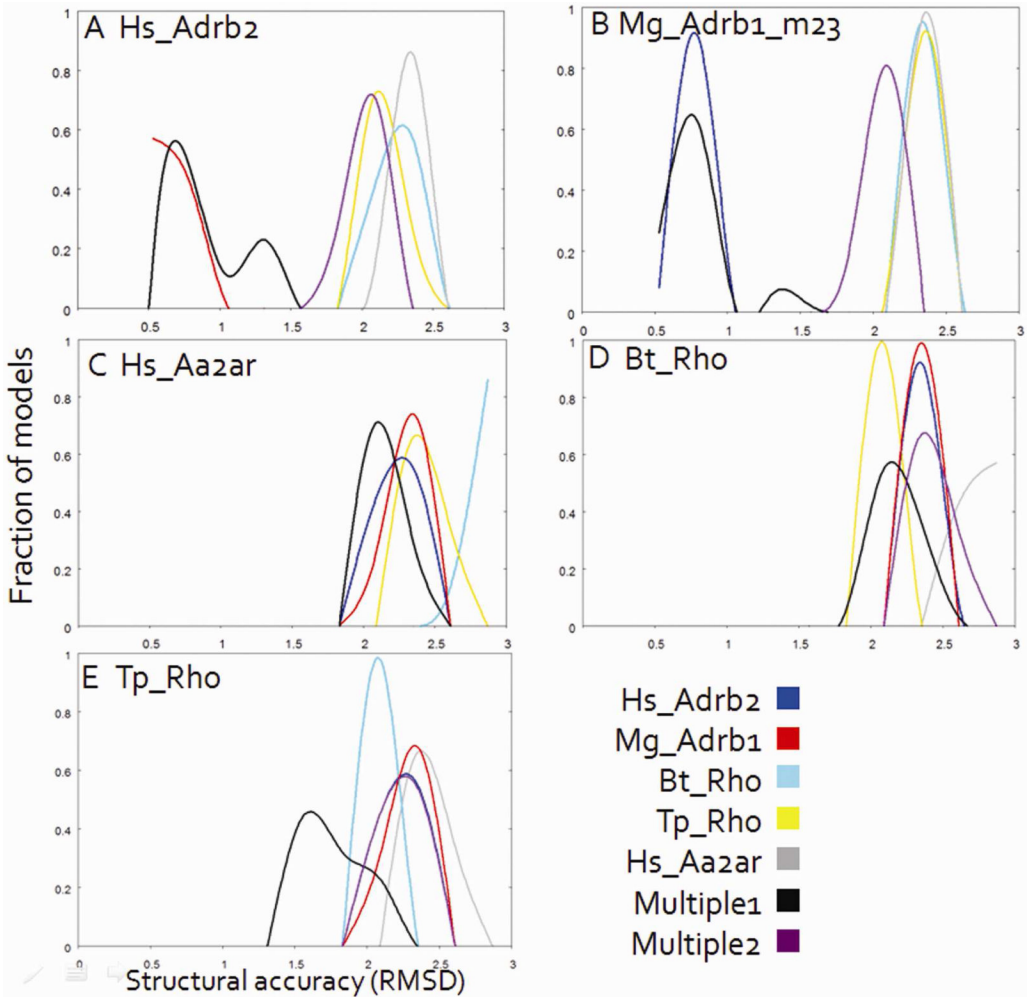

Figure 6.

A-E. Accuracy distribution of 1000 molecular models generated for each GPCR target with known crystal structure using single- or multiple-template homology modeling. The distribution of single-template models based on Bt_Rho, Tp_Rho, Mg_Adrb1_m23, Hs_Adrb2, and Hs_Aa2ar are shown in cyan, yellow, red, blue, and gray colors, respectively. Multiple templates were evaluated in the presence or absence of the crystal structures of highly homologous targets (Multiple 1 in black vs. Multiple2 in magenta).

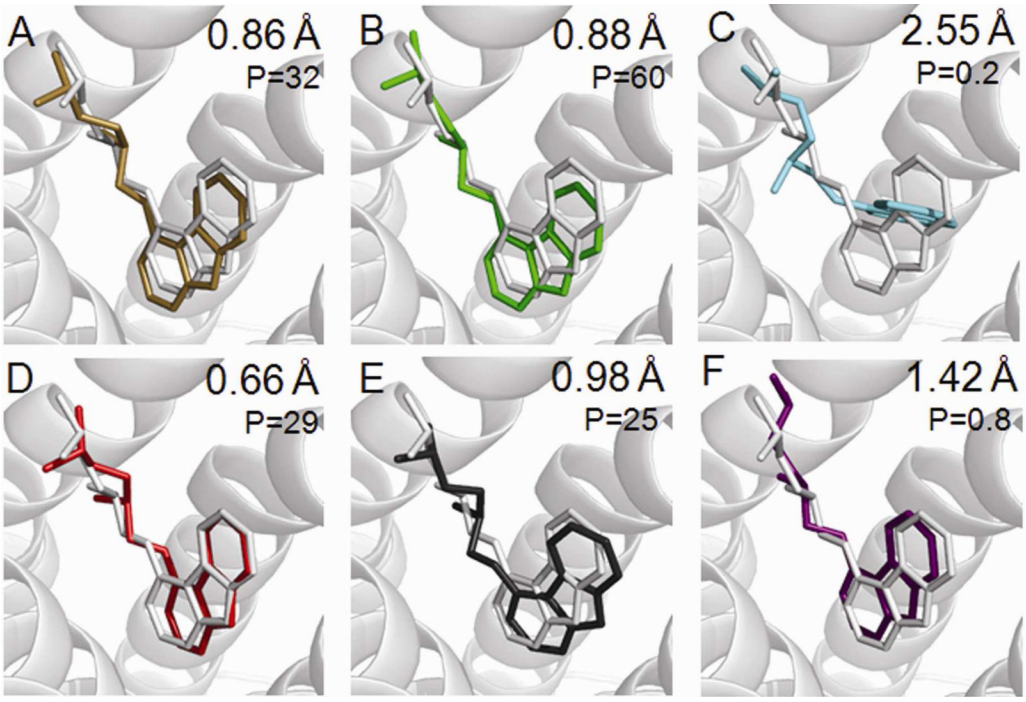

Figure 7.

Most accurate binding pose of carazolol docked into (A) Hs_Adrb2 crystal structure (brown), (B) Hs_Adrb2 crystal structure without loops (green), (C) a Bt_Rho based single-template model of Hs_Adrb2 (cyan), (D) a Mg_Adrb1_m23based single-template model of Hs_Adrb2 (red), (E) a multiple-template model with all available crystal structures but that of Hs_Adrb2 (Multiple 1, black), and (F) a multiple-template model with all available crystal structures but those of Hs_Adrb2 and the highly homologous receptor Mg_Adrb1_m23 (Multiple 2, magenta). Crystal structure of Hs_Adrb2 and carazolol are shown in white. The percentage P of obtaining a correct prediction is shown under the RMSD value for each model.

Table 1

iple-template homology models, respectively. Multiple templates either include all available crystal structures
available crystal structures but those of the target and its cognate receptor (Multiple2).

Single Template			Multiple-templates	
_Adrb2	Mg_Adrbl_m23	Hs_Aa2ar	Multiplel	Multiple2
21	20	23	45 { Tp_Rho, Hs_Adrb2, Mg_Adrb1_m23, Hs_Aa2ar }	30 { Hs_Adrb2, Hs_Aa2ar, Mg_Adrb1_m23 }
24	25	23	46 { Bt_Rho, Hs_Adrb2, Mg_Adrb1_m23, Hs_Aa2ar }	31 { Hs_Adrb2, Hs_Aa2ar, Mg_Adrb1_m23 }
-	68	35	77 { Bt_Rho, Tp_Rho, Mg_Adrb1_m23, Hs_Aa2ar }	48 { Bt_Rho, Tp_Rho, Hs_Aa2ar }

Single Template			Multiple-templates	
_Adrb2	Mg_Adrbl_m23	Hs_Aa2ar	Multiplel	Multiple2
68	-	35	76 [Bt_Rho, Tp_Rho, Hs_Adrb2, Hs_Aa2ar]	46 [Bt_Rho, Tp_Rho, Hs_Aa2ar]
35	35	-	-	50 [Bt_Rho, Tp_Rho, Hs_Adrb2, Mg_Adrb1]

Table 2

Structures and models used in molecular docking experiments with their respective templates.

Structure/Model name	Template(s)
Hs_Adrb2	-
Hs_Adrb2_no_loops	-
Hs_Adrb2_Rho	Bt_Rho
Hs_Adrb2_Adrb1	Mg_Adrb1_m23
Hs_Adrb2_Multiple1	Bt_Rho+Tp_Rho+ Hs_Aa2ar+Mg_Adrb1_m23
Hs_Adrb2_Multiple2	Bt_Rho+Tp_Rho+ Hs_Aa2ar